Materials Today Communications

In-situ synchrotron X-ray diffraction during quenching and tempering of SAE 52100 steel

--Manuscript Draft--

Manuscript Number:	MTCOMM-D-21-03098R1
Article Type:	Full Length Article
Section/Category:	Metals and alloys
Keywords:	SAE 52100 steel; Martensitic transformation; Lattice distortion; Synchrotron X-ray diffraction; Dilatometry
Corresponding Author:	Daniel Jon Foster The University of Manchester Manchester, UNITED KINGDOM
First Author:	Daniel Jon Foster
Order of Authors:	Daniel Jon Foster
	Mohan Paladugu
	Jonathan Hughes
	Maria Kapousidou
	Upol Islam
	Andreas Stark
	Norbert Schell
	Enrique Jimenez-Melero
Abstract:	The quenching and tempering process of SAE 52100 bearing steel was continuously monitored via in-situ dilatometry and high-energy X-ray diffraction, mapping the evolution of the constituent phases and lattice distortions and their direct correlation with observed dimensional changes of the material. During quenching from an austenitisation temperature of 860 °C to 50 °C, there was a continuous increase in lattice distortion in the parent austenite. Below the martensite start temperature of MS = 209 ± 15.0 °C, the c - lattice parameter and lattice distortion of the formed martensite initially decreased, then subsequently presented an increasing trend. An increase in sample length was detected only at martensite fractions ³ 18 vol.%, and occurred simultaneously with an increase in the ca'/aa' tetragonality ratio. An increase in sample length was detected during isothermal holding at 50 °C with a reduction in the martensite ca' parameter, potentially due to the expulsion of carbon. Tempering promoted the loss of martensite tetragonality at 283 ± 7.80 °C. At a tempering temperature of 340 °C, the austenite retained after quenching transformed completely within 1.5 min. The following reduction in sample length and expulsion of carbon from martensite is correlated to the relaxation of lattice distortion in the martensite-bainitic ferrite matrix.
Suggested Reviewers:	Carlos Garcia Mateo Spanish National Centre for Metals Research cgm@cenim.csic.es Area of expertise: processing and mechanical performance of advanced bainitic steel grades
	Adam Grajcar Silesian University of Technology adam.grajcar@polsl.pl Area of expertise: phase transformations and deformation mechanisms in high-strength steels with metastable austenite
	Minxin Huang The University of Hong Kong mxhuang@hku.hk

	Area of expertise: advanced high-strength steels, deformation mechanisms, crystal plasticity finite element modelling
	Mohammed Azeem University of Leicester ma812@leicester.ac.uk Area of expertise: in-situ synchrotron diffraction of advanced engineering alloys
Opposed Reviewers:	
Response to Reviewers:	

Manchester, 19th October 2021

Dear Editor,

We hereby submit the revised manuscript entitled *'In-situ synchrotron X-ray diffraction during quenching and tempering of SAE 52100 steel'* for publication in Materials Today Communications.

Outlined below in this cover letter is the list of changes made to the manuscript in response to the Editor and Reviewer comments.

Abstract - tense and language issues.
Abstract has been modified to use exclusively past tense language. Two sentences have been modified to read better.

Graphical abstract - low resolution, incorrect aspect ratio (should be 5x13).
Graphical abstract has been significantly reworked. The resolution has been increased and the aspect ratio is now 5 x 13.

Highlights - 85 characters maximum per bullet point (including spaces).
Highlights have been modified such that each is at a maximum of 85 characters (including spaces)

Please do not use first person 'we', 'our'.
All instances of the use of first person language have been replaced on pages: 4, 12, 16, 19 & 20, which are highlighted in yellow.

The tenses used in the manuscript are inconsistent. English language issues scattered throughout. We recommend making use of a reputable text editing service.
All references to variables and behaviours observed in the experiment have been changed to past tense, unifying the choice of tense. Present tense has been retained for explanations and discussion.
Language has been updated throughout the text which includes the rewriting of several passages and sentences and various smaller modifications, all in order to improve the quality of the written language. Such modifications are highlighted in green.
The author acknowledges the constructive advice on language (and, in particular, tense) and believes the manuscript reads more appropriately as a result.

We thank the editor in earnest for the comments and considerations and believe that, with the implementation of the suggested amended use of language, the revised manuscript is much improved.

Yours faithfully,

Daniel Foster

Mr. Daniel Foster
Department of Materials, University of Manchester,
Oxford Road, Manchester, M13 9PL, United Kingdom
Tel.: +44 (0)7908779706, email: daniel.foster-2@manchester.ac.uk

Highlights

1. At M_s = 209 °C, and increases in lattice distortion of martensite were observed.

2. Sample length and tetragonality only increase when ~18 vol.% of martensite formed.

3. Holding at the quench temperature, 2 vol.% of martensite formed and $c_{\alpha'}$ decreased.

4. Tetragonality disappeared at 283 °C when heating to the tempering temperature.

5. Austenite fully transformed into bainite after 1.5 min when tempering at 340 °C.

Graphical Abstract

The Quenching and Tempering of SAE 52100 steel

An in-situ synchrotron X-ray diffraction study

Beamline set up → *Martensite tetragonality and volume changes during quench*

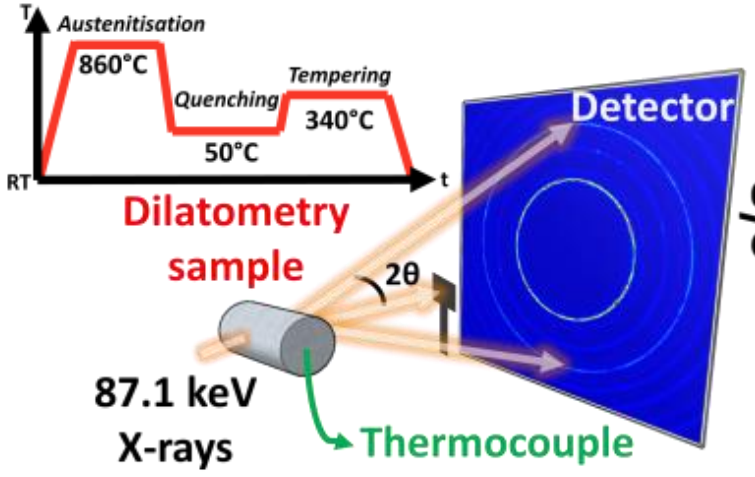

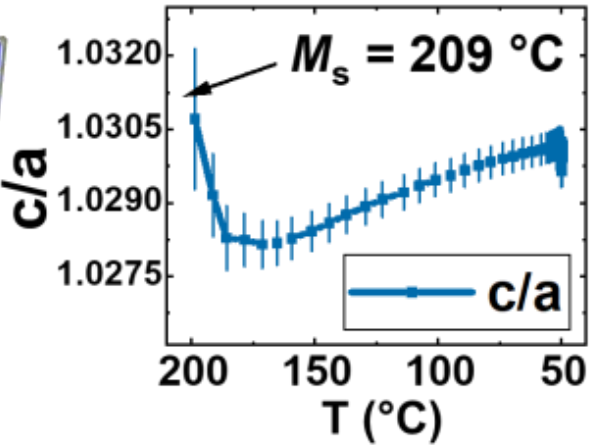

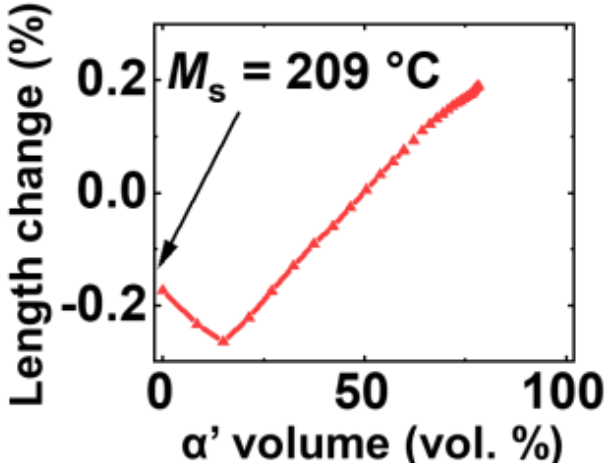

In-situ synchrotron X-ray diffraction during quenching and tempering of SAE 52100 steel

D. Foster[a,*], M. Paladugu[b,*], J. Hughes[a], M. Kapousidou[a], U. Islam[a], A. Stark[c], N. Schell[c],

E. Jimenez-Melero[a]

[a]*Materials Performance Centre, Department of Materials, The University of Manchester,*

M13 9PL, UK

[b]*The Timken Company World Headquarters (WHQ), North Canton, OH, 44720, USA*

[c]*Helmholtz-Zentrum Hereon, Max-Planck-Straße 1 I 21502 Geesthacht, Germany*

Corresponding authors (*):

daniel.foster-7@postgrad.manchester.ac.uk (DF)

mohan.paladugu@timken.com (MP)

Abstract

The quenching and tempering process of SAE 52100 bearing steel was continuously monitored via in-situ dilatometry and high-energy X-ray diffraction, mapping the evolution of the constituent phases and lattice distortions and their direct correlation with observed dimensional changes of the material. During quenching from an austenitisation temperature of 860 °C to 50 °C, there was a continuous increase in lattice distortion in the parent austenite. Below the martensite start temperature of M_S = 209 ± 15.0 °C, the c - lattice parameter and lattice distortion of the formed martensite initially decreased, then subsequently presented an increasing trend. An increase in sample length was detected only at martensite fractions ≥ 18 vol.%, and occurred simultaneously with an increase in the $c_{\alpha'}/a_{\alpha'}$ tetragonality ratio. An increase in sample length was detected during isothermal holding at 50 °C with a reduction in the martensite $c_{\alpha'}$ parameter, potentially due to the expulsion of carbon. Tempering promoted the loss of martensite tetragonality at 283 ± 7.80 °C. At a tempering temperature of 340 °C, the austenite retained after quenching transformed completely within 1.5 min. The following reduction in sample length and expulsion of carbon from martensite is correlated to the relaxation of lattice distortion in the martensite-bainitic ferrite matrix.

Keywords: SAE 52100 steel, martensitic transformation, lattice distortion, synchrotron X-ray diffraction, dilatometry

1. Introduction

Through-hardened SAE 52100 steel has been extensively used in the industrial production of high-precision bearings for decades [1, 2]. This hypereutectoid steel offers high machinability in the soft spheroidised-annealed state, along with high hardenability. The post-machining route of bearing components entails initial austenitisation at temperatures ≥ 840 °C, followed by oil quenching and water rinsing, and final tempering at 160–180 °C. This quench and tempering (QT) process yields a fine microstructure comprising tempered martensite, retained austenite (< 15 vol.%) and spherical Fe_3C particles (~2-3 vol.%) [2-4]. The as-manufactured bearing components offer high hardness (HRC 61–65) and high strength [1, 2]. During operation, the combined effect of Hertzian contact stresses and subsurface cyclic shear stresses, together with local higher temperatures at the contact, cause the phenomenon of rolling contact fatigue (RCF) [2, 5, 6]. The tolerance against RCF-induced damage normally dictates the service life expectancy of the bearing material [7]. Additionally, thermally induced and subsurface stress-induced transformation of the retained austenite into a body-centred cubic ferritic phase can lead to critical dimensional changes in bearing applications with strict tolerance requirements [4, 5, 8–11].

Tempering during manufacture or in higher-temperature service is expected to cause a loss of carbon in the martensite in the form of nano-scale carbides and a simultaneous reduction in the martensite's strength and retained austenite volume [12]. These phenomena suggest that microstructural changes have a significant influence on a bearing's dimensional alterations and service life. It is therefore of key importance to understand the mechanisms of phase transformations and the associated strengthening and dimensional change phenomena.

The steel's deformation history and heat treatment type and parameters affect the phase distribution, microchemistry and lattice defect structures, and thus determine the reference microstructural state of the steel bearing at the beginning of its service life as well as affecting

the through-life bearing performance. Microstructural changes in the steel during the bearing manufacturing stage, including heat treatment and machining at the (sub-) microscale, can lead to a significant dimensional alteration of bearing components [13]. In addition, the formation of martensite during steel quenching induces a higher dislocation density in both the parent austenite and the newly formed martensite, whereas the carbon content in martensite and its mechanical strength depend on the carbon content and grain size of the prior austenite [2, 14].

Simultaneously, changes in austenite fraction have been proposed as an additional area of study in the local damage evolution of bearing components [8]. Recent experimental reports point toward the solid solution strengthening of carbon atoms and other solutes in the predominant martensitic phase as a prime contributor to RCF resistance under white etching cracking damage conditions [15] and also to the mechanical stability of the retained austenite present in the microstructure [16].

Depth-resolved X-ray diffraction (XRD) is commonly used to assess the structural evolution of steel bearings [9, 11, 17-19]. The measured depth distributions of residual stresses and XRD peak widths of the martensitic reflections (e.g., $\{211\}_{\alpha'}$) reveal the generation of microplasticity and the evolution of lattice defects. In fact, the minimum full-width half-maximum (FWHM) ratio in the subsurface region prone to RCF damage with respect to the reference core structure serves as a link between bearing steel performance and mechanical engineering failure analysis of the bearing [17]. The reduction in martensitic FWHM during operation reveals a concomitant decrease in lattice distortion, which is attributed to glide-induced rearrangement of dislocations to lower energy configurations in the martensite [17].

In this work, phase and lattice strain evolution in bulk SAE 52100 steel were monitored in-situ during the QT heat treatment process using high-flux and high-energy synchrotron XRD. The goal of the presented work was to identify simultaneous changes in phase fractions, lattice parameter and lattice distortion. The QT treatment of high-carbon steels has been studied

via dilatometric, calorimetric and thermoelectric power measurements [20–22], ex-situ and recently in-situ, using low-flux and low-energy XRD [22]. The combined use of in-situ dilatometry and high-energy XRD in the QT processing of steels enabled the continuous temperature-time mapping of material volume changes via dilatometric measurements in relation to bulk phase evolution and atomic lattice level changes measured via XRD. This understanding may be useful in heat treatment process modelling and in-service predictions of bearing performance.

2. Experimental details

2.1 In-situ dilatometry

The starting material, with the chemical composition presented in Table 1, was received in the as-spheroidised condition. A cylindrical sample with a diameter of 4 mm and a length of 10 mm was machined from the stock material and inserted into a modified Bähr DIL 805 A/D dilatometer [23, 24], mounted on the P07 High Energy Materials Science Beamline [25] at PETRA III at the DESY synchrotron facility in Hamburg, Germany. An in-situ XRD experiment was performed in transmission geometry during a full QT cycle using a monochromatic beam of energy E = 87.1 keV (λ = 0.14235 Å) and a size of 0.5 mm^2 (Fig. 1a). The sample was induction-heated from room temperature to 860 °C at a rate of 3 °C/s, held at that temperature for 20 min, and subsequently helium gas-quenched to 50 °C at a rate of 60 °C/s. After 20 min at 50 °C, the sample was heated to 340 °C at a rate of 3 °C/s and held at that temperature for 120 min, and finally air-cooled to room temperature (Fig. 1b). The sample temperature was continuously monitored by a thermocouple spot welded onto the sample surface.

2.2 Data acquisition and analysis

During the sample quenching, two-dimensional diffraction patterns were collected at an acquisition rate of 1 Hz during heating and the majority of isothermal holding and increased to 10 Hz during quenching and for the first 10 min of isothermal holding after quenching using a PerkinElmer XRD 1621 flat panel detector at a distance of 1405 mm behind the sample. LaB_6 was used as the calibrant (Standard NIST Reference Material 660c). The recorded 2D dataset was integrated using the DAWN software package [26], and the resultant 1D patterns, as a function of temperature and time, were subsequently analysed using the Rietveld refinement method [27] implemented in the FullProf Suite software package [28].

Example 1D diffraction patterns are shown in Fig. 2a & b, where face-centred cubic austenite (γ) and orthorhombic cementite (Fe_3C) phases were detected during isothermal soaking of the steel at 860 °C, and body-centred tetragonal martensite (α') formed after quenching the steel to 50 °C (also shown in Fig. 2b). The Rietveld method was used for the refinement of the scale factor, phase fractions, lattice parameters and FWHM of the diffraction peaks of each phase present in the steel microstructure during the QT process. Each reflection was fitted with a pseudo-Voigt function in which FWHM and errors associated with phase volume fraction and lattice parameters were automatically extracted [27, 28].

2.3 Hardness and scanning electron microscopy measurements

To supplement the in-situ XRD observations, hardness measurements and microstructural characterisations were carried out on the as-quenched and subsequently tempered SAE 52100 steel. The steel was austenitised at 860 °C for 20 mins and quenched in an oil bath. The as-quenched samples were subjected to a standard industrial tempering treatment at 180 °C and another at 340 °C for different time durations. Metallographic samples were prepared from the as-quenched and quench-and-tempered (QT) steel and etched by a 2% nital solution. The microstructural morphology was characterised with an FEI Versa scanning electron microscope (SEM).

3. Results

3.1 Austenitisation

The relative change in the dilatometry sample length during the QT process is shown in Fig. 1c. This is a typical process for SAE 52100 steel in which the austenititsation time and temperature were selected to only partially dissolve carbides and prevent the quenched microstructure from becoming too coarse [2]. 50 °C was chosen as the quenching temperature to mimic industrial scale practices, with the elongated quenching time chosen likewise, but additionally and primarily to ensure temperature homogenisation through the sample. The high tempering temperature of 340 °C was chosen to accelerate the impact of tempering on the microstructure and dimensional changes within the experimental timeframe. During the initial sample heating at 3 °C/s for austenitisation, the ferrite matrix in the initial as-spheroidised microstructure (shown in Fig. S1 of the attached supplementary information) began to transform to austenite at A_{C1} = 760 ± 7.80 °C and completed the transformation at A'_{C1} = 809 ± 7.80 °C, as determined from X-ray diffraction data (Fig. 3a), whereas the sample length decreased by ~0.012 % (Fig. 3b) despite the increasing temperature. From the dilatometry data, concomitant changes were observed at 759 °C and 807 °C, respectively. Once the target temperature of 860 °C was reached and during the subsequent isothermal holding time of 20 min, a continuous reduction in Fe_3C volume fraction from f_{Fe3C} = 5.3 ± 0.2 vol.% to 3.1 ± 0.2 vol.% took place simultaneously with an increase in the austenite lattice parameter (Fig. 3c), and also an increase in the sample length of ~0.020 % (Fig. 3b).

A mass balance in the austenite-cementite region allows estimation of the carbon content in the austenite according to:

$$x_C^{\gamma} = \frac{\overline{x_C} - 6.67 \cdot f_{Fe3C}}{1 - f_{Fe3C}} \quad (1)$$

where the overall carbon content in the steel amounts to $\overline{x_C}$ = 1.005 wt.%. The cementite dissolution at 860 °C led to a change in carbon content in the austenite from $x_C^\gamma \sim 0.675\ wt.\%$ at t = 0 min to $x_C^\gamma \sim 0.830\ wt.\%$ at t = 20 min; i.e., an increase in carbon content of $\Delta x_C^\gamma \sim 0.155\ wt.\%$.

3.2 Quenching

The changes in the microstructure and sample length during helium gas quenching from 860 to 50 °C are presented in Fig. 4. From the XRD analysis, it was determined that the martensite start temperature, or M_s, in which martensite begins to form from austenite during the quenching is at a temperature of 209 ± 15.0 °C, considering the acquisition rate of 10 Hz and quench rate of 60 °C/s. The dilatometric measurement of the martensite start temperature was determined to be 189 °C. The first diffraction pattern acquired during quenching in which martensite was detected presented a volume fraction of 8.5 ± 0.4 vol.%. As such, the transformation behaviour of very low volume fractions of martensite (<9 vol.%) were undetectable within the time resolution of the experiment's acquisition rate. Since the austenite-to-martensite transformation is associated with a volume increase (FCC to BCC or BCT transformation), an increase in the dilatometer sample was expected around 209 °C. At the dilatometrically calculated M_s temperature of 189 °C, 15 ± 0.4 vol.% of martensite was detected. The volume fraction of Fe_3C remained constant throughout quenching and tempering within experimental resolution.

However, as can be seen in Fig. 4b, the dilatometer sample length continued to reduce under thermal contraction below M_S until $f_{\alpha'}$~18 vol.% formed. After $f_{\alpha'}$~18 vol.% had formed, the sample length increased continuously during cooling to a total of ~0.090 % when 50 °C was reached. The martensite volume fraction that will be formed at a selected quenching temperature (T_Q) below M_S can be estimated using the Koistinen-Marburger expression, empirically derived for carbon steels including SAE 52100 [29]:

$$f_{\alpha'} = 1 - \exp(-0.011\,(M_s - T_Q)) \quad (2)$$

Since the sample was quenched to T_Q = 50 °C, a martensite fraction of $f_{\alpha'}$ ~ 80 vol.% was expected to have formed at that temperature based on eq. (2). The XRD data analysis at 50 °C revealed a martensite fraction of $f_{\alpha'}$ = 79.1 ± 0.9 vol.%, together with an austenite fraction of f_γ = 19.6 ± 0.5 vol.% (Fig. 4a). The formed martensite was characterised by tetragonal symmetry at M_S and lower temperatures during quenching, as evidenced by the presence of the $\{101\}/\{110\}_{\alpha'}$ and the especially visible $\{002\}/\{200\}_{\alpha'}$ doublets in the 1D diffraction patterns (see Figs. 2 and 6a).

It is of interest to note from Fig. 4c that the $c_{\alpha'}$ decreased and $a_{\alpha'}$ increased slightly in the initial stages of the martensite formation. In addition, as can be seen in Fig. 4c, during cooling below M_S, the $c_{\alpha'}/a_{\alpha'}$ ratio in the martensite initially decreased with temperature but reached a minimum value at ~171 °C, the proceeded to increase during cooling as more martensite was formed. A similar trend was observed in the FWHM in the {310} martensite reflection (Fig. 4d), in which the FWHM reached a minimum value at ~186 °C. Moreover, the FWHM of the {311} austenite reflection increased continuously as the temperature decreased from M_S to 50 °C. Furthermore, during isothermal holding at a constant temperature of 50 °C for 20 min, a subtle continuous decrease in both $c_{\alpha'}$ and in a_γ was observed, but the martensite $a_{\alpha'}$ parameter remained constant (Figs. 5a and b). Over this time, an increase of 0.004% was observed in the sample length (Fig. 5c), together with an additional formation of ~2 vol.% martensite within the first 2 min at 50 °C.

3.3 Heating and tempering

During heating from 50 °C to the target tempering temperature of 340 °C, a subtle decrease in sample length was observed when the *Ms* temperature threshold of ~209 °C (Fig. 1c) was reached. A single 2D diffraction pattern was recorded during sample heating at the temperature T = 283 ± 7.80 °C, at which the measured austenite volume fraction was

~20 vol.% — largely unchanged from its value at 50 °C. In contrast, the martensite lattice presented cubic symmetry at 283 °C within the experimental resolution, as opposed to the detectable tetragonal symmetry at 50 °C before the start of tempering (see Fig. 6a). Upon reaching 340 °C, an austenite fraction of only f_γ ~12 vol.% remained, which fully transformed into a body-centred cubic phase (henceforth referred to as α) within 1.5 min from the start of the isothermal holding period (see Figs. 6b and 7a). To distinguish between phases in the microstructure during different sections of the heat treatment, this work denotes the body-centred tetragonal martensite formed during quenching as α', and the BCC tempered martensite and lower bainite matrix formed during tempering as α; ferrite present in the as-spherioidised state before austenitisation is also denoted as α.

During this transformation time at 340 °C, a continuous increase in the austenite lattice parameter and in FWHM of the $\{311\}_\gamma$ reflection was detected (Figs. 7b and 7c). Conversely, the cubic lattice parameter of the martensite phase decreased steadily over this time, concomitantly with a gradual reduction in the $\{310\}_\alpha$ FWHM during austenite transformation (Figs. 7b and 7c). At longer durations, when the austenite transformation was completed, the $\{310\}_\alpha$ FWHM continued to decrease steadily, together with a reduction in the sample length of ~0.005 % (Fig. 8).

3.4 Hardness and morphology

Four samples in differently tempered states were obtained for ex-situ measurements. A sample tempered at an industry standard temperature of 180 °C for 1 hour was chosen as a comparative benchmark sample to compare microstructural evolution characteristics with the accelerated high temperature sample. Fig. 9 shows the hardness plot of the SAE 52100 steel in the as-quenched and in the quenched and differently tempered states. In the as-quenched state, a hardness value of ~67 HRC was measured. After tempering for 1.5 hr at 180 °C, the hardness reduced to ~63 HRC. When the quenched steel was tempered at 340 °C, the hardness reduced

to ~56 HRC; no significant difference in hardness was evident with tempering time (1 hr vs. 2 hr) at 340 °C. The microstructural morphology of the steel with respect to the tempering, as revealed by etching the polished steel surface with a 2% nital solution, is shown in Fig. 10.

The SEM micrograph in the as-quenched state (Fig. 10a) did not reveal many nano-scale or microstructural features other than carbide particles. With tempering at 180 °C for 1.5 hr, a fibre (nonwoven) or feather-like morphology appeared (Fig. 10b). Islands of retained austenite are visible with tempering at 180 °C for 1.5 hr (Fig. 10b). Higher-temperature tempering at 340 °C showed rod-like carbide morphologies (Figs. 10c and 10d). With an increase in tempering time to 2 hr (Fig. 10d), a slight decrease in the aspect ratio of carbides was observed, but otherwise, no considerable difference in microstructure morphology was noted with longer tempering times at 340 °C (1 hr vs. 2 hr; Figs. 10c and 10d, respectively).

4. Discussion

4.1. Austenitisation and carbide dissolution at 860 °C

The as-spheroidised microstructure was heated at a rate of 3 °C/s and soaked isothermally at 860 °C for 20 min. The measured temperature range for ferrite-to-austenite phase transformation at that heating rate was A_{c1} = 760 ± 7.80 °C to A'_{c1} = 809 ± 7.80°C, in which the transformation was detected via X-ray diffraction at A_{c1} = 760 ± 7.80 °C and completed at A'_{c1} = 809 ± 7.80 °C. These values are consistent with the change in behaviour of the dilatometry curves which presented changes at 759 °C and 807 °C, respectively. Ferrite-to-austenite transformation involves crystal structure transformation of BCC to FCC. Since the FCC lattice arrangement has a greater atomic packing density than the BCC lattice, the volume of the material tends to decrease with the ferrite-to-austenite transformation. Thus, this transformation was accompanied by a decrease in the dilatometry sample length of ~0.12%.

In literature on similar steels, a heating rate of 2 °C/s is reported to yield the temperature values of A_{C1} = 753 °C and A'_{C1} = 789 °C [30], confirming the dependence of those critical values on the heating rate for a given Cr content and the initial spheroidised microstructure (which determines the soluble carbon content) in the steel [31]. Thermodynamic calculations revealed full cementite dissolution at temperatures > 870 °C. The presence of other carbides such as M_7C_3 or $M_{23}C_6$ (M = Fe, Cr) were not detected for this 1.46 wt.% Cr steel grade within experimental resolution [32].

During soaking at 860 °C, the asymptotic increase in the austenite lattice parameter and simultaneous increase in the sample length (Figs. 3b and c) are related to the cementite dissolution from f_{Fe3C} = 5.3 ± 0.2 vol.% to 3.1 ± 0.2 vol.% and the consequent carbon enrichment of the austenite matrix. The concentration slope at the cementite-austenite interface is the controlling parameter of the process, with a strong coupling of the C and Cr diffusion at the interface [30]. The driving force decreases with the cementite content present at a given time in the microstructure, and in these tests, equilibrium was not reached after the 20 min isothermal holding step at 860 °C. There remained ~3 vol.% Fe_3C in the microstructure, and the resultant carbon content in the austenite matrix amounted to $x_C^\gamma \sim 0.830\ wt.\%$. Thermocalc software estimates based on a pseudo-binary phase diagram predict a somewhat higher carbon content in austenite of $x_C^\gamma \sim 0.88\ wt.\%$ at the soaking temperature of 850 °C for 45 min [33].

4.2. Martensite formation during quenching to 50 °C

After 20 min of isothermal holding at 860 °C, the sample was He gas-quenched to 50 °C at a cooling rate of 60 °C/s. The pre-existing austenite with a volume fraction of 97 vol.% and an average carbon content of $x_C^\gamma \sim 0.830\ wt.\%$ gradually transformed into tetragonal martensite as the temperature was reduced from M_S = 209 ± 15.0 °C to 50 °C (Fig. 4a). At the lowest temperature, an austenite fraction of f_γ = 19 vol.% remained untransformed.

The austenite-to-martensite transformation involved a volume expansion of ~4% [34]. This is reflected in a subtle change in gradient in the temperature dependence of the austenite lattice parameter at the M_S temperature (Fig. 4c), with a higher rate of reduction in the lattice parameter with temperature in the martensite formation regime. This higher rate of reduction in the austenite lattice parameter suggests the build-up of isostatic compressive stresses in the austenite, possibly applied from the surrounding martensite formation that accompanied the volume expansion within the steel's microstructure. The austenite-to-martensite transformation-induced volume expansion is known to cause an increase in sample length; some part of the expansion itself leads to the development of stresses within the microstructure. However, an increase in overall sample length with decreasing temperature was detected experimentally only after 18 vol.% of martensite had formed at 189 °C (Fig. 4b). In addition, the $c_{\alpha'}/a_{\alpha'}$ ratio in the martensite reached a minimum at 171 °C, and at lower temperatures, it increased steadily to attain a value of ~1.030 at 50 °C (Fig. 3c).

It is of interest to note from Figs. 4c and 4d that the $c_{\alpha'}$, $c_{\alpha'}/a_{\alpha'}$ ratio and FWHM$\{310\}_{\alpha'}$ decreased during the initial stages of the martensite formation, and then proceeded to increase with a greater volume of the formed martensite. In addition, there was also slight increase in $a_{\alpha'}$ during initial stages of the martensite formation (Fig. 4c). This observation of the martensite transformation is consistent with the shear mechanism of martensite formation (also known as Bain lattice distortion) [35]. Martensite formation is understood to be a displacive phase transformation, meaning atoms do not diffuse with respect to neighbouring atoms, instead displacing by a shear mechanism. During the shear mechanism, $c_{\alpha'}$ forms by the contraction of a_γ by 20% [$(c_{\alpha'} - a_\gamma) / a_\gamma \approx -20\%$] and $a_{\alpha'}$ forms by expanding half of the face diagonal to the γ phase by 12% [$(a_{\alpha'} - (a_\gamma/\sqrt{2})) / (a_\gamma/\sqrt{2}) \approx 12\%$]. The initial decrease of $c_{\alpha'}$ and increase of $a_{\alpha'}$ are possibly due to this expansion and contraction during the phase formation stage until the characteristic dimensions are acquired. The data in Fig. 4c matches with these Bain strain

results except "$(c_{\alpha'} - a_\gamma) / a_\gamma$" varies between -18.1% to -18.5%, and "$(a_{\alpha'} - (a_\gamma/\sqrt{2})) / (a_\gamma/\sqrt{2})$" varies between 12 to 12.45. This decreased contraction (a_γ to $c_{\alpha'}$) and increased expansion ($a_\gamma/\sqrt{2}$ to $a_{\alpha'}$) may be related to a higher content of entrapped interstitial carbon in the lattice. The initial decrease in the peak broadness of the $\{310\}_{\alpha'}$ reflection in Fig. 4d may also be related to this shear mechanism of martensite formation. The variations in the Bain strains as more martensite formed is shown in supporting material, Figure S3.

In martensitic Fe-C steels containing > 0.6 wt.%C, the trapped interstitial C content, located preferentially in one of three potential sub-lattices of octahedral interstices in the martensite lattice, affects the tetragonal $c_{\alpha'}/a_{\alpha'}$ ratio according to the Honda and Nishiyama equation [34,36-38]:

$$c_{\alpha'}/a_{\alpha'} = 1.000 + 0.045 \cdot x_C^{\alpha'} \quad (3)$$

This expression yields a value of $x_C^{\alpha'} \sim 0.67\ wt.\%$ at 50 °C, but does not directly take into account the potential impact of the dislocation/twin substructure in martensite on the $c_{\alpha'}/a_{\alpha'}$ ratio [39]. It is expected that during cooling below M_S, the austenite grains with lower thermal stability — i.e., low-carbon grains — will transform first [40], and higher-carbon austenite grains will be destabilised as the undercooling below M_S increases.

An average carbon content in the prior austenite phase at 860 °C of $x_C^{\gamma} \sim 0.830\ wt.\%$ implies the formation of mixed lath/plate martensite morphologies upon quenching based on the presence of Fe-C alloys [41]. In this study, lower-magnification SEM observations suggest lath-like martensite morphologies (as shown in Fig. S2 of the supporting information). During martensite transformation by the shear mechanism and also due to the constraint of the surrounding austenite, the newly formed martensite units undergo a lattice invariant deformation through slip and twinning. When slip dominates the martensite deformation mechanism, dislocations are introduced both at the martensite-austenite interface and within the martensitic units [41]. The dislocation density in lath martensite, and also the probability

of twin formation, are reported to increase with the amount of carbon retained in the tetragonal lattice as the microstructure is cooled below M_S [41, 42]. This leads to an enhanced lattice distortion in the martensite, as evidenced by the increase in the FWHM $\{310\}_{\alpha'}$ during cooling, which occurred simultaneously with the build-up of lattice defects in the remaining austenite and the corresponding increase in the FWHM $\{311\}_{\gamma}$ (see Fig. 4d). In addition, as shown in Figs. 4c and 4d, the increases in $c_{\alpha'}$ and FWHM $\{310\}_{\alpha'}$ (after the initial decrease), may suggest the rest of the untransformed austenite was enriched in carbon and/or higher-carbon containing austenite grains started to transform. Therefore, the newly formed martensite exhibited increased lattice strains. Consequently, the average lattice distortion of martensite, realised in the FWHM of the $\{310\}_{\alpha'}$ reflection, showed an increasing trend after an initial decrease.

It is of interest note that the M_s temperature determined by XRD is 209 ± 15.0 °C, but the dilatometry sample began to show an increase in length only after ~18 vol.% of martensite had formed. This result suggests that a considerable fraction of phase transformation is required to observe bulk volumetric growth in the material.

Once the lowest temperature of 50 °C was reached, there was a subtle increase in sample length at a rate that decreased after approximately 1 min of isothermal holding at that temperature. The early stage of isothermal holding also coincided with the formation of an additional ~2 vol.% martensite and with a progressive reduction in the lattice parameter of the untransformed austenite, stemming from the build-up of additional isostatic compressive stresses in the austenite due to the transformation itself. Moreover, the martensite present in the microstructure experienced a continuous decrease in the $c_{\alpha'}$ parameter, whereas the $a_{\alpha'}$ parameter remained constant for the entire 20 min at 50 °C (Fig. 5). The decrease in the $c_{\alpha'}$ parameter at 50 °C can be attributed to rearrangement and clustering of carbon atoms in the octahedral sites of the BCC lattice and to the dislocations and interfaces within the microstructure, which are known to occur at temperatures ≤ 100 °C [43].

However, when the steel was held at 50 °C, martensite could initiate its tempering and form a small fraction of intermediate carbides - primarily hexagonal ε-carbide ($Fe_{2.4}C$) - though such carbides could not be detected within experimental resolution. Carbon can redistribute to low-energy sites associated with dislocations, vacancies or lath boundaries during low-temperature tempering [44–48], therefore also affecting the strength of the martensite [14]. The carbon segregation from the supersaturated tetragonal lattice and the nano-sized carbide formation could lead to the observed continuous reduction in the $c_{\alpha'}$ parameter of martensite during isothermal holding at 50 °C, and consequently to the subtle increase in sample length.

4.3. Tempering at 340 ℃

The as-quenched microstructure, after holding for 20 min at 50 °C, was heated to 340 °C at a rate of 3 °C/s and held at that temperature for 120 min. During heating, the gradual loss of tetragonality that started at 50 °C continued, and at 283 ± 7.80 °C the tetragonal distortion within the martensite lattice was undetectable (Fig. 6). In this first stage of tempering where the loss of tetragonality occurs, nm-sized transition carbides are expected to form [34, 41, 49, 50]. At 283 °C, 19 vol.% of austenite remained intact in the microstructure. However, once the target temperature of 340 °C was reached, only 12 vol.% austenite was detected.

Metastable austenite is reported to transform isothermally into bainitic ferrite in the temperature range of ~200–300 °C [5, 45, 47, 51]. Lower bainite is expected to form preferentially at temperatures lower than 350 °C in SAE 52100 steel [52]. In these experiments, at 340 °C the remaining 12 vol.% austenite transformed within only 1.5 min (Fig. 7). Though the austenite appeared stable before it became undetectable within experimental resolution, the ultra-low volume fractions of austenite introduced a large uncertainty in the measured volume fraction values. During that period, the untransformed austenite experienced an increase in both its lattice parameter and in the FWHM of the $\{311\}_{\gamma}$ reflection. These facts evidence the

increase in the average austenite carbon content, and simultaneously in the lattice distortion, due to the isostatic internal compressive stresses applied from the surrounding newly formed martensite.

The newly formed bainitic ferrite was expected to contain a carbon content close to its maximum solubility. The previously measured activation energy for the austenite decomposition in the SAE 52100 steel pointed at carbon diffusion in austenite ahead of the moving austenite-bainitic ferrite interface as the limiting step controlling the austenite transformation [5, 53, 54]. Additionally, any excess in carbon in the body-centred cubic lattice of martensite would be released as carbides. At this temperature, cementite particles would preferentially form, initially with a needle-like morphology, and potentially with a prior dissolution of the intermediate carbide particles formed at 50 °C and during heating of the material to 340 °C [45, 47, 55].

As a consequence of this process, the a_α parameter decreased and stabilised after approx. 1 min at 340 °C, but the FWHM of $\{310\}_\alpha$ decreased steadily from the start of isothermal holding at 340 °C, and continued this trend beyond the first 1.5 min, when the austenite transformation was completed and the carbon release from the martensite and bainitic ferrite lattice took place. Simultaneously, the carbon release during the tempering step resulted in precipitation of transition carbides and iron carbides (Fe_2C, $Fe_{2.7}C$ and Fe_3C). This relaxation of the internal lattice distortion occurred up to the maximum holding time of 120 min, and reflected itself in the simultaneous reduction in sample length (Fig. 8). The final value of the FWHM of $\{310\}_\alpha$ after 120 min of tempering at 340 °C was still much higher than that of the ferrite matrix in the spheroidised-annealed state (Fig. 8). Typically, the spheroidisation annealing treatment is carried out in the range of 800 to 700 °C for significantly longer times, and hence the resultant ferrite phase tends have equilibrium characteristics. Therefore, the

tempered martensite at 340 °C still showed higher FWHM of $\{310\}_\alpha$ compared to the ferrite phase of the spheroidised-annealed microstructure.

The effect of tempering was visible in the observed hardness decrease with increasing tempering temperature (Fig. 9). This effect was amplified at 340 °C as with 1 hr tempering, hardness reduced to ~56 HRC, and a further increase in tempering time to 2 hr did not result in considerable hardness reduction. Both hardness values obtained after tempering at 340 °C were lower than the hardness measured in the standard 180 °C temper. As the BCC iron lattice underwent a reduction in carbon content and associated lattice distortion, the steel exhibited a loss of hardness. As seen in Fig. 8, there was a considerable decrease in the FWHM of the $\{310\}_\alpha$ reflection in the initial stages of martensite tempering at 340 °C, but in later stages (after the first 30 min), there was no considerable decrease in the lattice strain. The hardness decrease also showed a similar trend (Fig. 9).

The microstructural morphological changes shown in Fig. 10 suggest how tempering affects the etching of steel and, consequently, the microstructural morphology. In the as-quenched state (Fig. 10a), the microstructure is under inherent isostatic stresses and hence did not show considerable localised etching differences. Consequently, the microstructural morphology was not visible except for the presence of carbide particles. Since carbide particles generally etch at a much slower rate (or simply do not etch at all) compared to the surrounding matrix by the Nital solution, only the carbide particles were visible (Fig. 10a). These round carbide particles are thought to be remnants from the initial spheroidised state of the steel (Fig. S1), which were not dissolved completely during austenitisation at 860 °C. With tempering at 180 °C (Fig. 10b), the martensite lattice is in the process of losing carbon, hence the microstructure showed localised etching differences, and as a consequence presented a fibre (nonwoven) or feather-like morphology which includes nano-sized transition carbides.

In general, microstructural areas depleted of carbon showed deeper etching and a darker appearance in the images. With the tempering temperature increase to 340 °C, spatially dispersed rod-like carbide morphologies appeared, suggesting that a larger area was deeply etched due to the loss of carbon from the martensite. Typically, at temperatures above 300 °C, ε-carbides tend to dissolve and rod-shaped cementite particles precipitate and grow. As tempering time increases, the rod shaped carbide particles tend to show a reduction in aspect ratios in order to form as spheroids within the tempering time [56].

5. Conclusions

The bulk microstructural evolution of SAE 52100 bearing steel was monitored in-situ through the quenching and tempering process using high-energy X-ray diffraction. During quenching from the austenitisation temperature of 860 °C down to 50 °C, austenite started to transform into martensite at M_S = 209 ± 15.0 °C, and the remaining austenite experienced significant local compressive stresses and lattice distortions that increased in magnitude with the amount of martensite formed. However, a significant increase in sample length and in the $c_{\alpha'}/a_{\alpha'}$ tetragonality ratio was only detected when ~18 vol.% martensite had formed at the lower temperature of 171 °C. It is observed that, in accordance with the Bain distortion model, the lattice parameters of the martensite phase changed with respect to the parent austenite phase. The lattice distortion of the formed martensite decreased during its initial formation stage and then exhibited an increasing trend.

During isothermal holding at 50 °C, an additional 2 vol.% martensite was generated from the remaining austenite, and the $c_{\alpha'}$ parameter decreased continuously during the 20 min holding time, signalling the early stage of carbon segregation and potential formation of intermediate carbides. There was simultaneously a subtle increase in sample length at that temperature. This process of interstitial carbon expulsion from the martensite tetragonal lattice

was accelerated during the subsequent heating, and the martensite tetragonality could no longer be experimentally detected by synchrotron X-ray diffraction at 283 ± 7.80 °C. Moreover, the metastable austenite fully transformed into bainitic ferrite after only 1.5 min at the highest tempering temperature of 340 °C. This transformation occurred concomitantly with a gradual reduction in the a_α lattice parameter and in the FWHM of the $\{310\}_\alpha$ reflection. The change in sample length observed beyond that period of 1.5 min is correlated with the progressive relaxation of lattice distortion in the tempered martensite-plus-bainitic ferrite matrix.

Acknowledgements

This work was made possible by financial support and samples provided by The Timken Company. The PETRA III synchrotron facility at DESY (Germany) are acknowledged for the time granted on the P07 beam line under the proposal I-20180929 EC. Chris Akey, Matt Hillard, Greg Kissiar and Bob Pendergrass of the TIMKEN WHQ are acknowledged for assisting with quench & tempering and microstructure characterization of 52100 steel.

References

[1] E.V. Zaretsky, *Rolling bearing steels – a technical and historical perspective*, Mater. Sci. Technol. 28 (2012) 58-69.
[2] H.K.D.H. Bhadeshia, *Steels for bearings*, Prog. Mater. Sci. 57 (2012) 268-435.
[3] A. da S. Rocha, T. Hirsch, *Fast in situ X-ray diffraction phase and stress analysis during complete heat treatment cycles of steel*, Mater. Sci. Eng. 395 (2005) 195-207.
[4] E. Jimenez-Melero, R. Blondé, M.Y. Sherif, V.Honkimäki, N.H.van Dijk, *Time-dependent synchrotron X-ray diffraction on the austenite decomposition kinetics in SAE 52100 bearing steel at elevated temperatures under tensile stress*, Acta Mater. 61 (2013) 1154-1166.
[5] E. Jimenez-Melero, R. Blondé, M.Y. Sherif, V. Honkimäki, N.H. van Dijk, *Time-dependent synchrotron X-ray diffraction on the austenite decomposition kinetics in SAE 52100 bearing steel at elevated temperatures under tensile stress*, Acta Mater. 61 (2013) 1154-1166.
[6] F. Sadeghi, B. Jalalahmadi, T. Slack, N. Raje, N.K. Arakere, *A Review of Rolling Contact Fatigue*, J. Tribol. 131 (2009) 041403.
[7] R. L. Widner, *Failures of Rolling-Element Bearings* in *ASM Handbook: Volume 11: Failure Analysis and Prevention* ed. by W.T. Becker and R.J. Shipley. ASM Int. (2009) 490.
[8] A. Voskamp. *Microstructural changes during rolling contact fatigue*. PhD thesis, Delft University of Technology, The Netherlands, 1997.
[9] R.C. Dommarco, K.J. Kozaczek, P.C. Bastias PC, G.T. Hahn, C.A. Rubin, *Residual stresses and retained austenite evolution in SAE 52100 steel under non-ideal rolling contact loading*, Wear 257 (2004) 1081-1088.

[10] C. Sidoroff, M. Perez, P. Dierickx, D. Girodin. *Advantages and Shortcomings of Retained Austenite in Bearing Steels: A Review* in *ASTM Special Technical Publication STP 1580* (2015) 312.
[11] M. Paladugu, R.S. Hyde, *Influence of microstructure on retained austenite and residual stress changes under rolling contact fatigue in mixed lubrication conditions*, Wear. 406-407 (2018) 84.
[12] J. Hidalgo, K.O. Findley, M.J. Santofimia, *Thermal and mechanical stability of retained austenite surrounded by martensite with different degrees of tempering*, Mater. Sci. Eng A 690 (2017) 337-347
[13] .H.W. Zoch, *Distortion engineering: Vision or ready to application?* Materialwissenschaft u. Werkstofftech. 40(5-6) (2009) 342-348.
[14] C.H. Young, H.K.D.H. Bhadeshia, *Strength of mixtures of bainite and martensite*, Mater. Sci. Technol. 10 (1994) 209-214.
[15] M. Paladugu, R. Scott Hyde, *Material composition and heat treatment related influences in resisting rolling contact fatigue under WEC damage conditions*, Int. J. Fatigue. 134 (2020) 105476.
[16] D. Foster, M. Paladugu, J. Hughes, M. Kapousidou, C. Barcellini, D. Daisenberger, E. Jimenez-Melero, *Comparative micromechanics assessment of high-carbon martensite/bainite bearing steel microstructures using in-situ synchrotron X-ray diffraction*, Mater. 14 (2020) 100948.
[17] J. Gegner, *Tribological Aspects of Rolling Bearing Failures*, in: C.H. Kuo (Ed.), *Tribology. Lubricants and Lubrication*, IntechOpen, 2011
[18] A.P. Voskamp, R. Österlund, P.C. Becker, O. Vingsbo, *Gradual changes in residual stress and microstructure during contact fatigue in ball bearings*, Met. Technol. 7 (1980) 14.
[19] R.H. Vegter, H.A. Verschoor, A. Girones, *X-ray microdiffraction for the analysis of bearing operation conditions*, ASTM Int. 3 (7) (2006) JAI14058.
[20] L. Cheng, C.M. Brakman, B.M. Korevaar, E.J. Mittemeijer, *The tempering of iron-carbon martensite; dilatometric and calorimetric analysis*, Metall. Trans. A 19A (1988) 2415-2426.
[21] M. Perez, C. Sidoroff, A. Vincent, C. Esnouf, *Microstructural evolution of martensitic 100Cr6 bearing steel during tempering: From thermoelectric power measurements to the prediction of dimensional changes*, Acta Mater. 57 (2009) 3170-3181.
[22] M. Hunkel, J. Dong, J. Epp , D. Kaiser, S. Dietrich, V. Schulze, et al., *Comparative Study of the Tempering Behavior of Different Martensitic Steels by Means of In-Situ Diffractometry and Dilatometry*, Materials 13 (2020) 5058.
[23] P. Staron, T. Fischer, T. Lippmann, A. Stark, S. Daneshpour, D. Schnubel, et al. *In Situ Experiments with Synchrotron High-Energy X-Rays and Neutrons*, Adv. Eng. Mater. 13 (2011) 658-663.
[24] N. Schell, *Synchrotron-Based Capabilities for Studying Engineering Materials at PETRA-III*, Synch. Rad. News 30 (2017) 29-34.
[25] N. Schell, A. King, F. Beckmann, H.U. Ruhnau, R. Kirchhoff, R. Kiehn, et al., *The High Energy Materials Science Beamline (HEMS) at PETRA III*, AIP Conf. Proc. 1234 (2010) 391.
[26] J. Filik, A.W. Ashton, P.C.Y. Chang, P.A. Chater, S.J. Day, M. Drakopoulos, et al., *Processing two-dimensional X-ray diffraction and small-angle scattering data in DAWN 2*, J. Appl. Cryst. 50 (2017) 959-966.
[27] R.A. Young, *The Rietveld Method*. IUCr Monographs on Crystallography, Oxford University Press, 1993.
[28] J. Rodríguez-Carvajal, *Recent Advances in Magnetic Structure Determination by Neutron Powder Diffraction*, Phys. B 192 (1993) 55.

[29] D.P. Koistinen, R.E. Marburger, *A general equation prescribing the extent of the austenite-martensite transformation in pure iron-carbon alloys and plain carbon steels*, Acta Metall. 7 (1959) 59-60.
[30] L. Zhao, F.J. Vermolen, A. Wauthier, J. Sietsma, *Cementite Dissolution at 860°C in an Fe-Cr-C Steel*, Metall. Mater. Trans A 37A (2006) 1841.
[31] J.M. Beswick, *The effect of chromium in high carbon bearing steels*, Metall. Trans A 18 (1987) 1897-1906.
[32] L.R. Woodyatt, G. Krauss, *Iron-chromium-carbon system at 870°C*, Met. Trans. A 7A (1976) 983-989.
[33] J. Epp, H. Surm, O. Kessler, T. Hirsch, *In situ X-ray phase analysis and computer simulation of carbide dissolution of ball bearing steel at different austenitizing temperatures*. Acta Mater. 55 (2007) 5959-5967.
[34] D.A. Porter, K.E. Easterling, M.Y. Sherif, *Phase Transformations in Metals and Alloys*, 3rd ed., Taylor & Francis, 2009.
[35] M. S. Wechsler, D. S. Lieberman, and T. A. Read:Trans. AIME, 1953, vol. 197, p. 1503.
[36] Z. Nishiyama, *Martensitic transformation*, Academic Press, 1978.
[37] Y. Lu, H. Yu, R.D. Sisson Jr., *The effect of carbon content on the c/a ratio of as-quenched martensite in Fe-C alloys*, Mater. Sci. Eng. A 700 (2017) 592-597.
[38] N. Maruyama, S. Tabata, H. Kawata, *Excess Solute Carbon and Tetragonality in As-Quenched Fe-1Mn-C (C:0.07 to 0.8 Mass Pct) Martensite*, Metall. Trans. A 51 (2020) 1085-1097.
[39] S. Kajiwara, T. Kikuchi, *On the abnormally large tetragonality of martensite in Fe-Ni-C alloys*, Acta Metall. Mater. 39(6) (1991) 1123-1131.
[40] E. Jimenez-Melero, N.H. van Dijk, L. Zhao, J. Sietsma, S.E. Offerman, J.P. Wright, S. van der Zwaag, *Martensitic transformation of individual grains in low-alloyed TRIP steels*, Scripta Mater. 56 (2007) 421-424.
[41] G. Krauss, *Steels. Processing, Structure, and Performance*, 2nd ed., ASTM, 2015.
[42] S. Morito, J. Nishikawa, T. Maki, *Dislocation Density within Lath Martensite in Fe–C and Fe–Ni Alloys*, ISIJ Int. 43(9) (2003) 1475-1477.
[43] G. Krauss, *Microstructures, Processing, and Properties of Steels*, Properties and Selection: Irons, Steels, and High-Performance Alloys, Vol 1, ASM Handbook, By ASM Handbook Committee, ASM International (1990) 126-139.
[44] M.K. Miller, P.A. Beaven, G.D.W. Smith, *A study of the early stages of tempering of iron-carbon martensites by atom probe field ion microscopy*, Metall. Trans. A 12 (1981) 1197-1204.
[45] W.C. Leslie, *The physical metallurgy of steel*, McGraw-Hill, 1982.
[46] G. Krauss, *Martensite in steel: Strength and structure*, Mater. Sci. Eng. A 273-275 (1999) 40-57.
[47] M. Jung, S.J. Lee, Y.K. Lee, *Microstructural and Dilatational Changes during Tempering and Tempering Kinetics in Martensitic Medium-Carbon Steel*, Metall. Mater. Trans. A 40 (2009) 551-559.
[48] A. Vieweg, E. Povoden-Karadeniz, G. Ressel, P. Prevedel, T. Wojcik, F. Mendez-Martin, et al., *Phase evolution and carbon redistribution during continuous tempering of martensite studied with high resolution techniques*. Mater. Des. 136 (2017) 214-222.
[49] T.A. Balliet, G. Krauss, *The effect of the first and second stages of tempering on the microcracking in martensite of an Fe-1.22 C alloy*, Metall Trans. 7 (1976) 81-86.
[50] K. Han, M.J. van Genderen, A. Böttger, H.W. Zandbergen, E.J. Mittemeijer, *Initial stages of Fe-C martensite decomposition*, Philos. Mag. 81 (2001) 741.
[51] G.R. Speich, W.C. Leslie, Tempering of steel, Metall. Trans. 3 (1972) 1043-1054.
[52] G.E. Hollox, R.A. Hobbs, J.M. Hampshire, *Lower bainite for adverse environments*, Wear 68 (1981) 229-240.

[53] C. Wells, W. Batz, R.F. Mehl, Diffusion coefficient of carbon in austenite, JOM 2 (1950) 553-560.
[54] R.W. Neu, H. Sehitoglu, *Transformation of Retained Austenite in Carburised 4320 Steel*, Metall. Trans. A 22A (1991) 1491-1500.
[55] M.J. van Genderen, M. Isac, A. Böttger, E.J. Mittemeijer, *Aging and Tempering Behaviour of Iron-Nickel-Carbon and Iron-Carbon Martensite*, Metall. Mater. Trans. A 28A (1997) 545-561.
[56] S. Yamasaki, Modelling Precipitation of Carbides in Martensitic Steels, Doctoral Thesis, University of Cambridge (2004)

Tables

Table 1. Chemical composition (wt.%) of the SAE 52100 steel used in this study.

C	Cr	Mn	Si	Cu	Ni	Al	Fe
1.005	1.46	0.32	0.27	0.19	0.1	0.024	Bal.

Figure Captions

Fig. 1. (a) Schematic representation of the high-energy synchrotron X-ray diffraction experiment performed in combination with dilatometry. An X-ray beam with a size of 0.5 mm^2 and an energy of 87.1 keV (λ = 0.14235 Å) illuminated the centre of the cylindrical sample. (b) Schematic temperature-time diagram of the QT treatment performed in situ at the synchrotron beamline. (c) The relative change in sample length during the experiment. The measured values for the critical austenitisation temperatures (A_{C1}, A'_{C1}) and the martensite start temperature (M_s), determined via X-ray diffraction are labelled.

Fig. 2. (a) The Rietveld analysis of a 1D diffraction pattern after 20 min soaking at 860 °C, and (b) a plot representing the 1D diffraction pattern right after quenching the sample to 50 °C. The two green rows of vertical lines correspond to (a) (top tow) orthorhombic cementite (Fe_3C) and (bottom row) face-centred cubic austenite (γ), and in (b), austenite, body-centred tetragonal martensite (α') and cementite are represented by the vertical green lines, respectively.

Fig. 3. (a) Temperature dependence of the ferrite (red) and austenite (blue) volume fractions during heating above 700 °C to the target soaking temperature of 860 °C. (b) The relative change in sample length as a function of the austenite volume fraction in the same temperature range as (a). (c) Austenite lattice parameter (blue, left *y*-axis), and volume fraction of Fe_3C (grey, right *y*-axis) as a function of the soaking time up to 20 min at 860 °C.

Fig. 4. (a) Temperature variation of the transforming austenite and the newly formed martensite during quenching at 350 to 50 °C, together with (b) the relative change in sample length as a function of martensite volume fraction, the temperature evolution of (c) the austenite (a_γ) and martensite ($a_{\alpha'}$, $c_{\alpha'}$) lattice parameters, and (d) the FWHM of the $\{311\}_\gamma$ reflection (blue) and $\{310\}_{\alpha'}$ reflection (red). The inset in (c) corresponds to the martensite $c_{\alpha'}/a_{\alpha'}$ ratio as a function

of temperature. The FWHM of the $\{310\}_{\alpha}$ reflection measured in the spheroidised-annealed state at 50 °C before austenitisation (red triangle) is also plotted as reference.

Fig. 5. (a) Lattice parameters of martensite ($a_{\alpha'}$, $c_{\alpha'}$) as a function of time during isothermal holding at 50 °C after quenching the sample from the soaking temperature of 860 °C; (b) time dependence of the austenite lattice parameter (a_{γ}). (c) Relative change in sample length and corresponding volume fraction of martensite during isothermal holding at 50 °C. The acquisition time of the 2D detector was 10 Hz for the quenching and first 10 minutes of isothermal holding, and thereafter reduced to 1 Hz. Error bars are omitted every 10 data points for clarity. The step seen between the acquisition rates is a product of change in intensity due to exposure time.

Fig. 6. Evolution of the (a) $\{002\}/\{200\}_{\alpha'}$ martensite doublet and (b) $\{200\}_{\gamma}$ austenite reflection at selected temperatures and times during heating of the sample from 50 to 340 °C and isothermal holding at the latter temperature.

Fig. 7. Time evolution during isothermal holding at 340 °C of (a) the austenite volume fraction until it becomes undetectable within experimental uncertainty, (b) the lattice parameters of α-phase (red) and γ-phase, and (c) the FWHM of the $\{310\}_{\alpha}$ and $\{311\}_{\gamma}$ reflections.

Fig. 8. Relative change in sample length and in FWHM of the $\{310\}_{\alpha}$ reflection for the entire isothermal tempering of 120 min at 340 °C. The dotted line denotes the FWHM of the $\{310\}_{\alpha}$ reflection as measured in the as-spheroidised condition.

Fig. 9. Rockwell hardness (HRC) of the SAE 52100 steel in the as-quenched sample and in post-quench with different stages of tempering.

Fig. 10. Scanning electron microscope (SEM) micrographs showing microstructural morphology of SAE 52100 steel in the as-quenched sample and in post-quench with different tempering stages. The metallographic samples were prepared from the steel and etched with 2% nital solution.

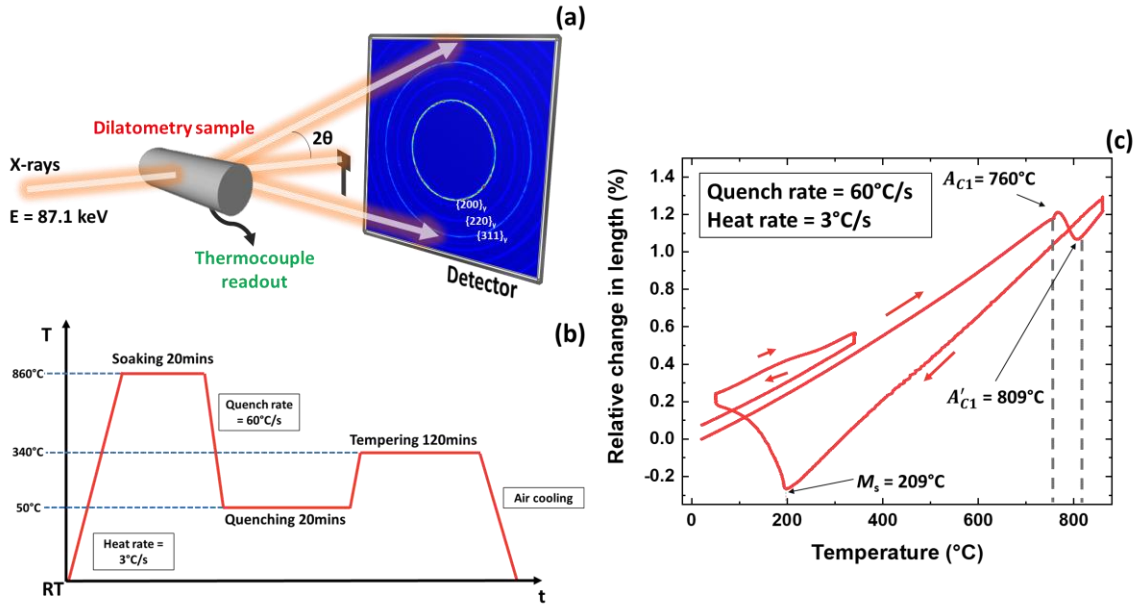
(a)
Dilatometry sample
X-rays
E = 87.1 keV
2θ
Thermocouple readout
Detector
{200}γ
{220}γ
{311}γ
(b)
T
860°C
340°C
50°C
RT
t
Soaking 20mins
Quench rate = 60°C/s
Tempering 120mins
Air cooling
Quenching 20mins
Heat rate = 3°C/s
(c)
Quench rate = 60°C/s
Heat rate = 3°C/s
A_{C1} = 760°C
A'_{C1} = 809°C
M_s = 209°C
Relative change in length (%)
Temperature (°C)

Fig. 1

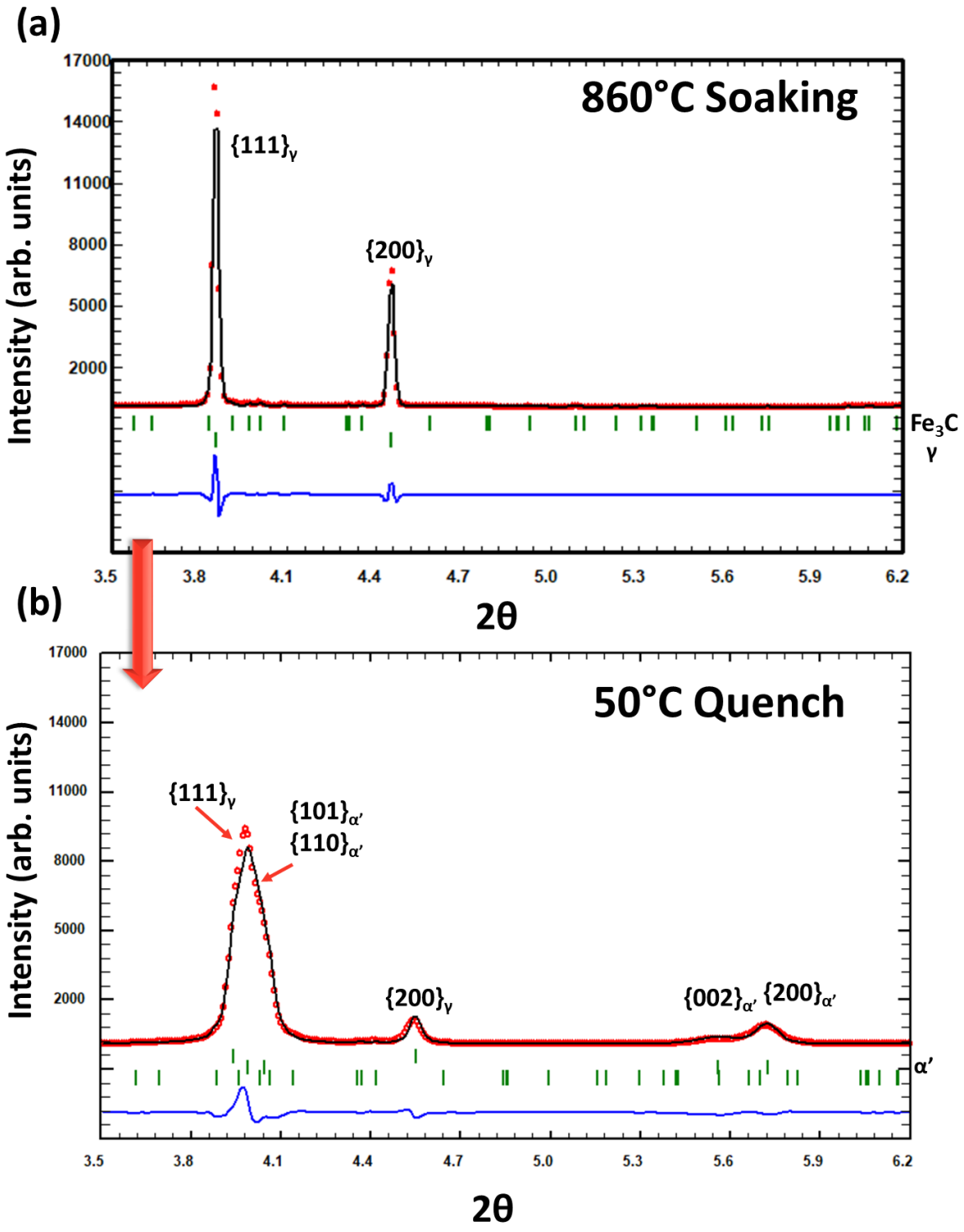
(a)
860°C Soaking
Intensity (arb. units)
{111}γ
{200}γ
Fe3C
γ
2θ
(b)
50°C Quench
Intensity (arb. units)
{111}γ
{101}α′
{110}α′
{200}γ
{002}α′ {200}α′
α′
2θ

Fig. 2

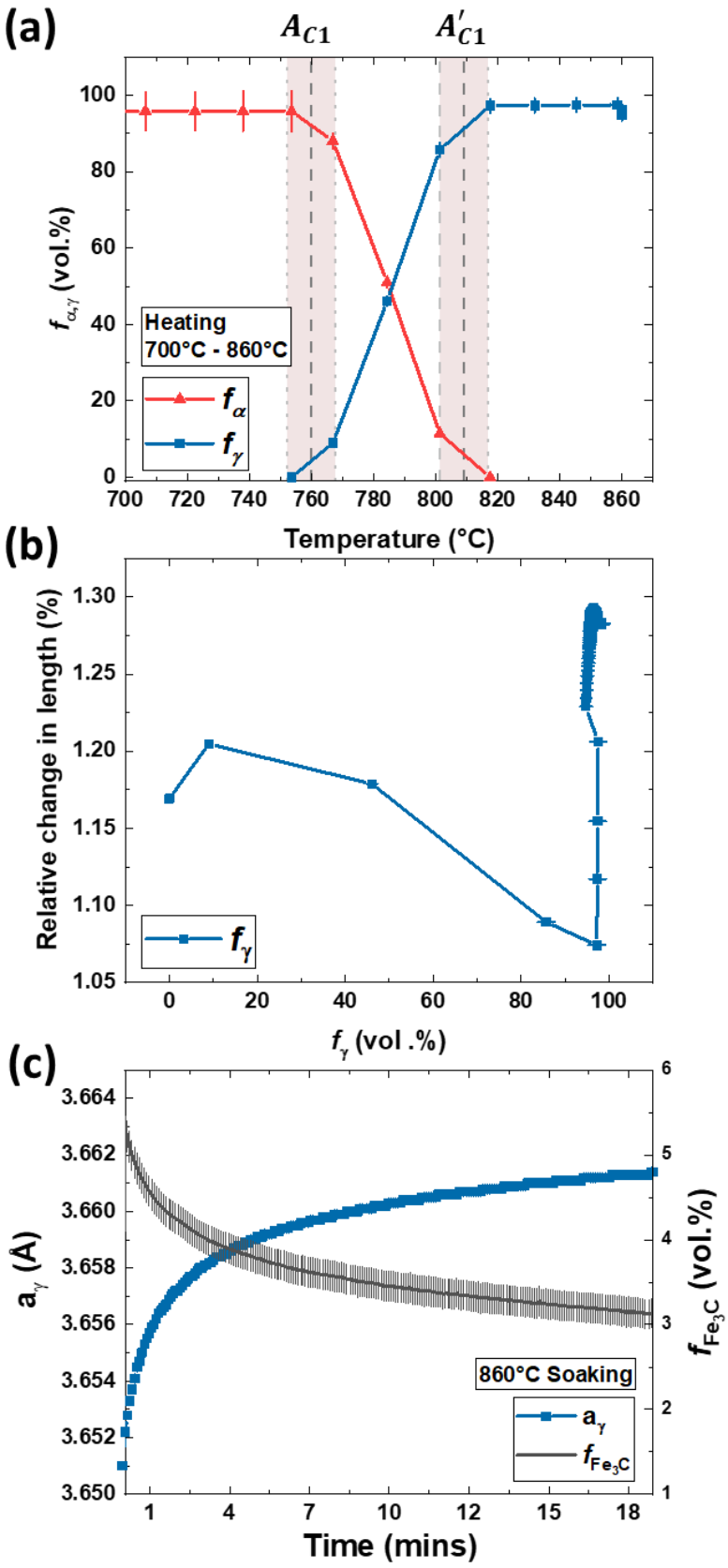
(a)
A_{C1}
A'_{C1}
$f_{\alpha,\gamma}$ (vol.%)
Heating
700°C - 860°C
f_α
f_γ
Temperature (°C)
(b)
Relative change in length (%)
f_γ
f_γ (vol .%)
(c)
a_γ (Å)
f_{Fe_3C} (vol.%)
860°C Soaking
a_γ
f_{Fe_3C}
Time (mins)

Fig. 3

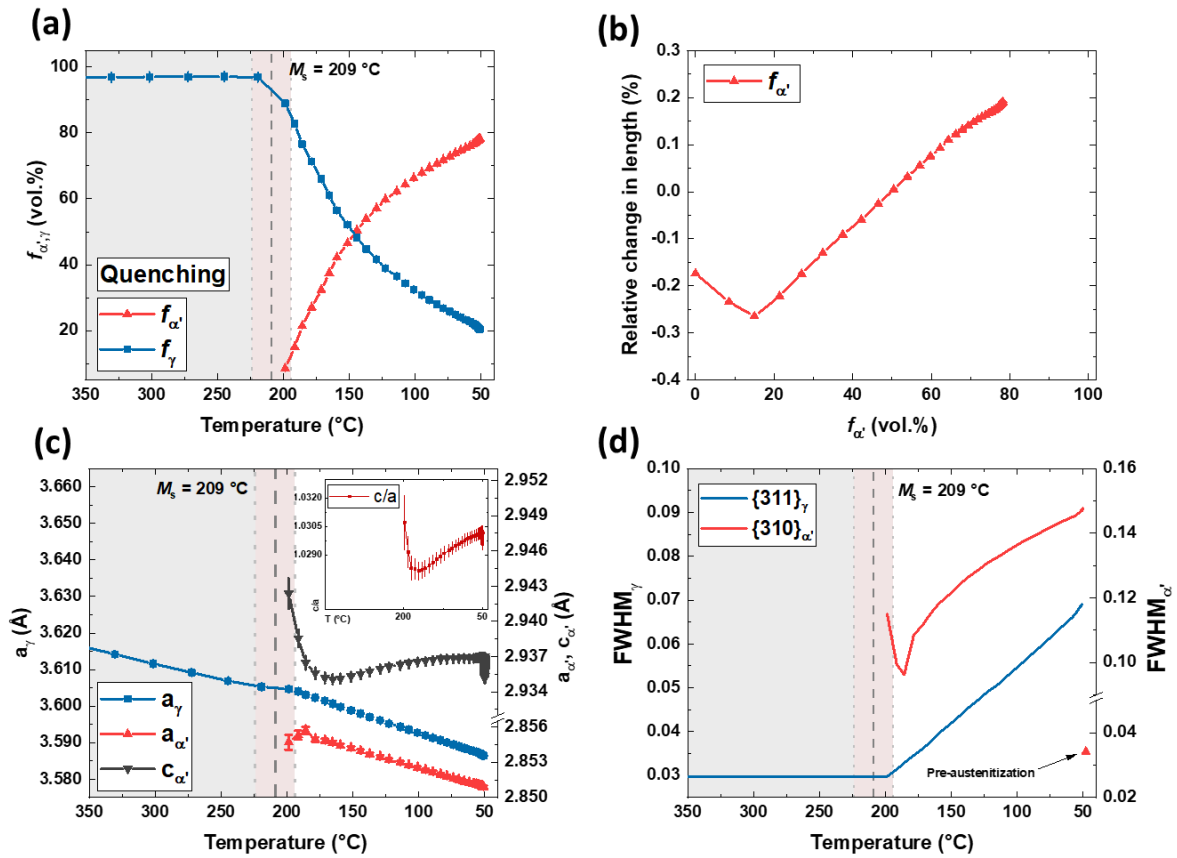
(a)
M_s = 209 °C
Quenching
$f_{\alpha'}$
f_γ
$f_{\alpha',\gamma}$ (vol.%)
Temperature (°C)
(b)
$f_{\alpha'}$
Relative change in length (%)
$f_{\alpha'}$ (vol.%)
(c)
M_s = 209 °C
c/a
T (°C)
a_γ
$a_{\alpha'}$
$c_{\alpha'}$
a_γ (Å)
$a_{\alpha'}$, $c_{\alpha'}$ (Å)
Temperature (°C)
(d)
{311}$_\gamma$
{310}$_{\alpha'}$
M_s = 209 °C
FWHM$_\gamma$
FWHM$_{\alpha'}$
Pre-austenitization
Temperature (°C)

Fig. 4

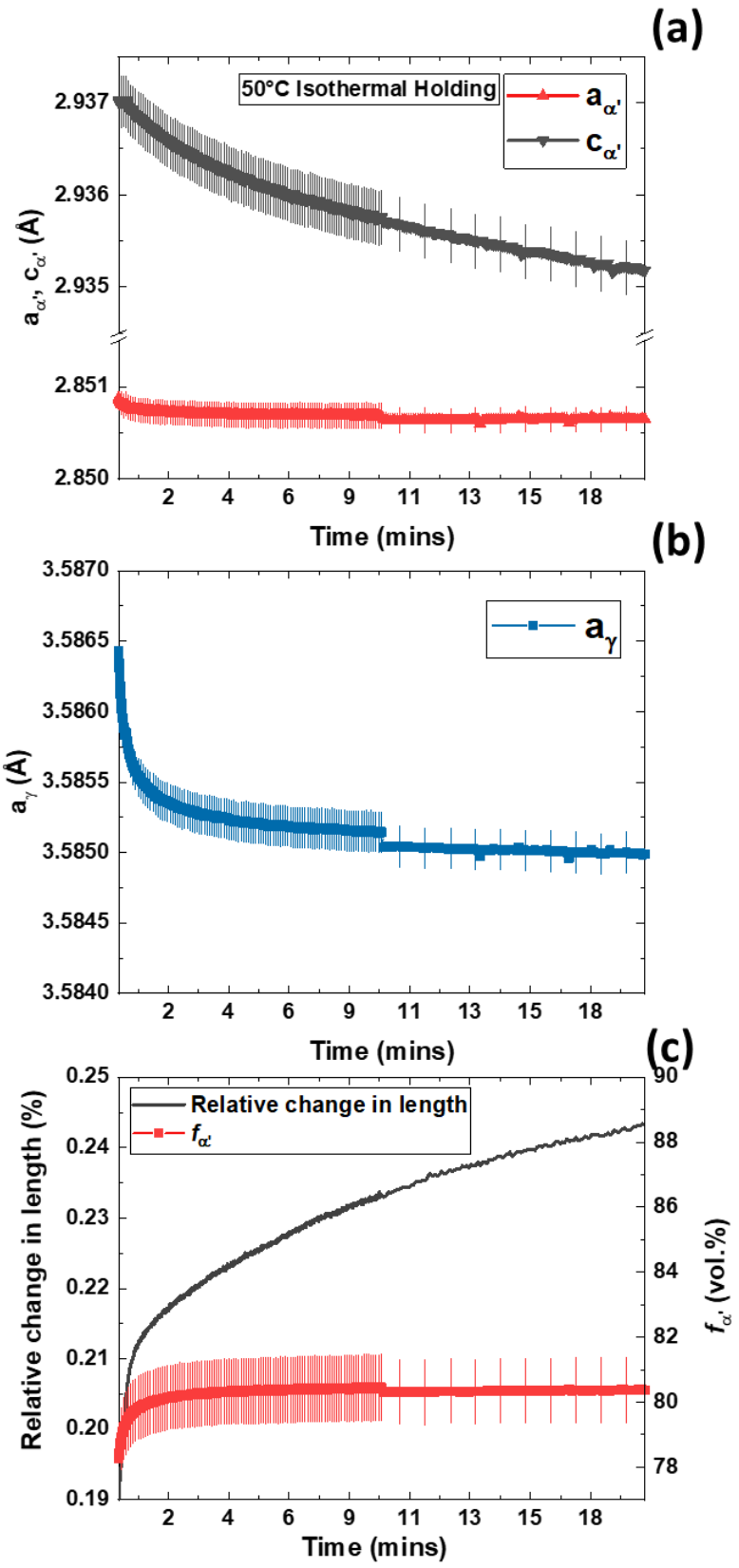
(a)
50°C Isothermal Holding
$a_{\alpha'}$
$c_{\alpha'}$
$a_{\alpha'}$, $c_{\alpha'}$ (Å)
2.937
2.936
2.935
2.851
2.850
2 4 6 9 11 13 15 18
Time (mins)
(b)
a_{γ}
a_{γ} (Å)
3.5870
3.5865
3.5860
3.5855
3.5850
3.5845
3.5840
2 4 6 9 11 13 15 18
Time (mins)
(c)
Relative change in length
$f_{\alpha'}$
Relative change in length (%)
0.25
0.24
0.23
0.22
0.21
0.20
0.19
90
88
86
84
82
80
78
$f_{\alpha'}$ (vol.%)
2 4 6 9 11 13 15 18
Time (mins)

Fig. 5

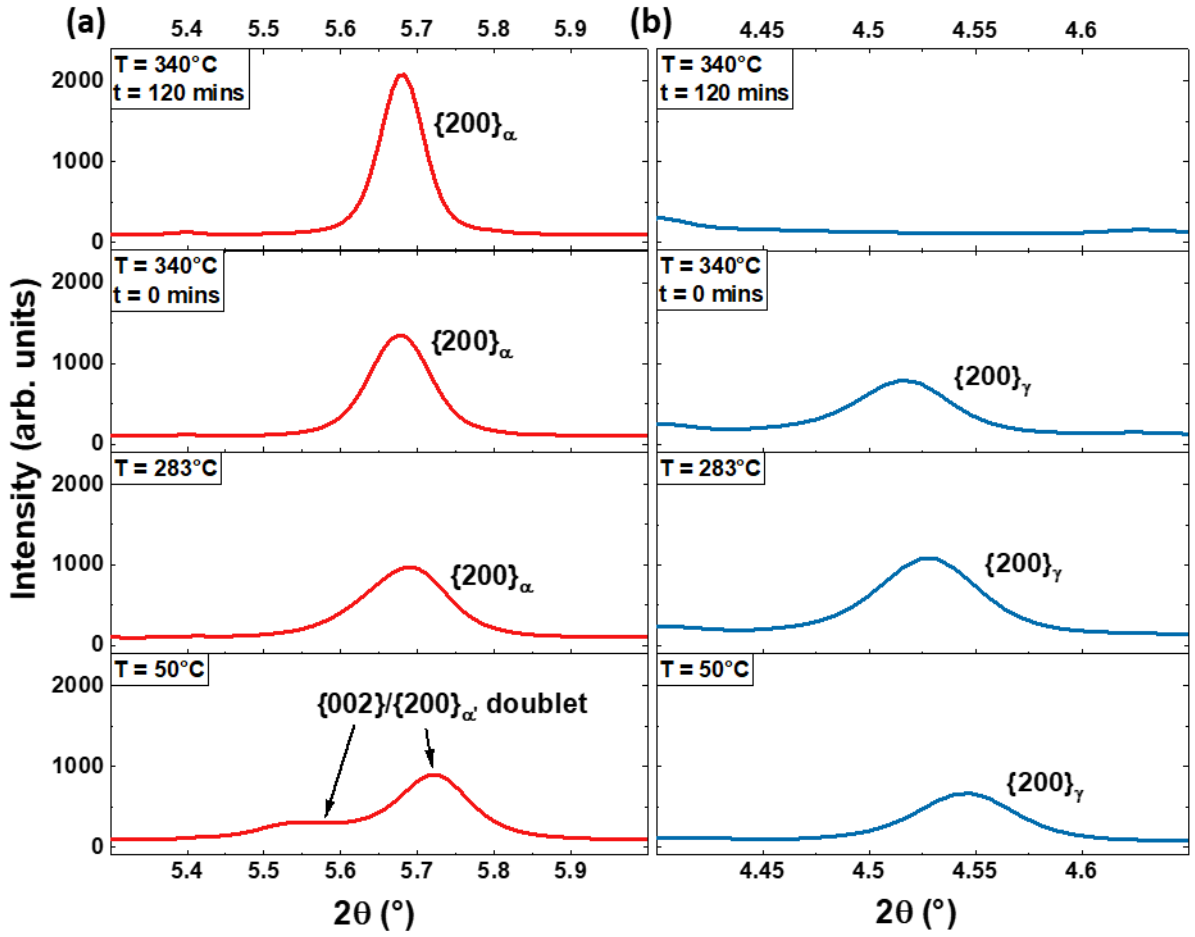
(a)
(b)
T = 340°C
t = 120 mins
{200}α
T = 340°C
t = 0 mins
{200}α
T = 283°C
{200}α
T = 50°C
{002}/{200}α' doublet
T = 340°C
t = 120 mins
T = 340°C
t = 0 mins
{200}γ
T = 283°C
{200}γ
T = 50°C
{200}γ
Intensity (arb. units)
2θ (°)
2θ (°)

Fig. 6

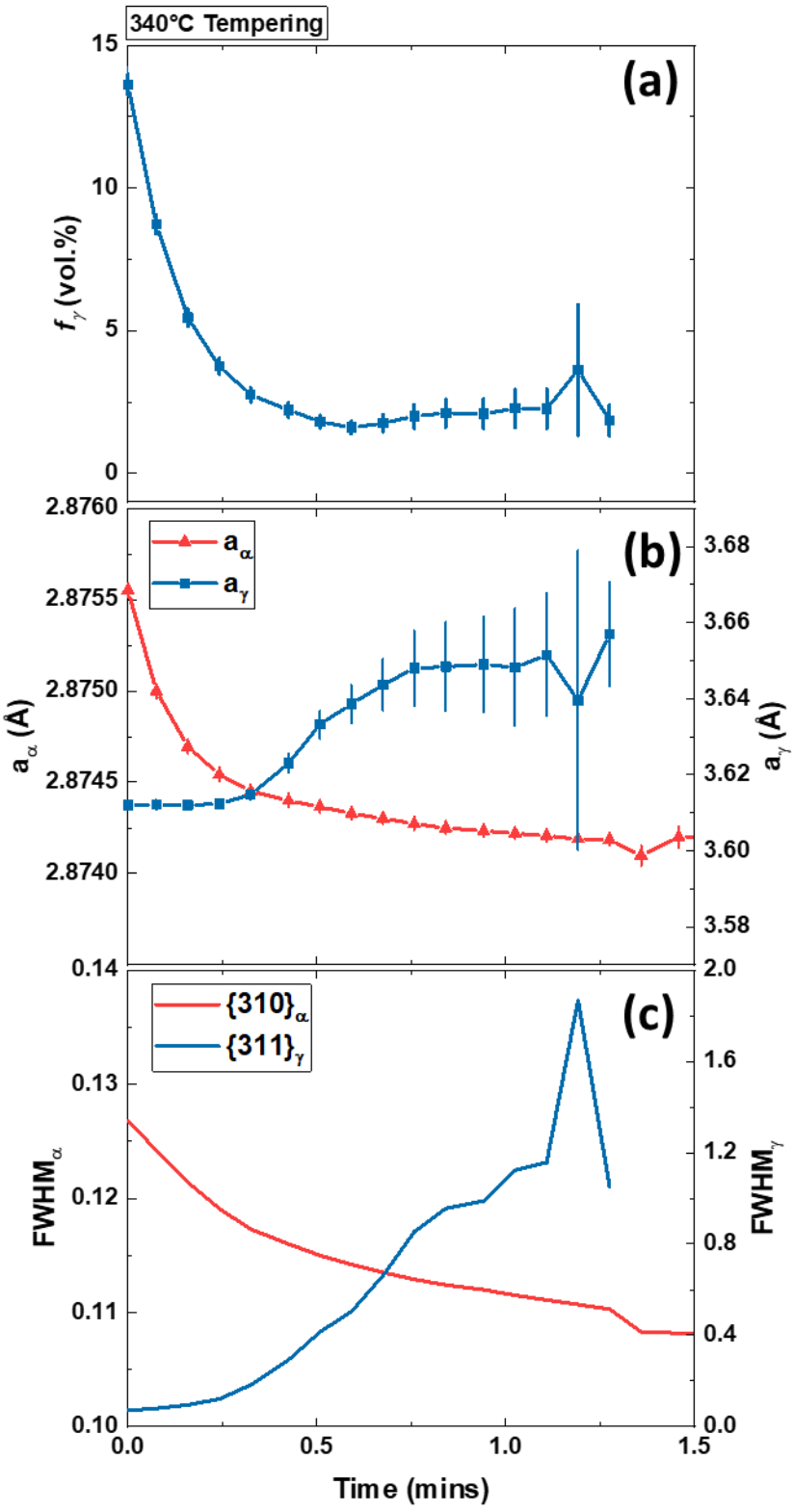
340°C Tempering
(a)
f_γ (vol.%)
15
10
5
0
(b)
a_α
a_γ
a_α (Å)
a_γ (Å)
2.8760
2.8755
2.8750
2.8745
2.8740
3.68
3.66
3.64
3.62
3.60
3.58
(c)
{310}$_\alpha$
{311}$_\gamma$
FWHM$_\alpha$
FWHM$_\gamma$
0.14
0.13
0.12
0.11
0.10
2.0
1.6
1.2
0.8
0.4
0.0
0.0
0.5
1.0
1.5
Time (mins)

Fig. 7

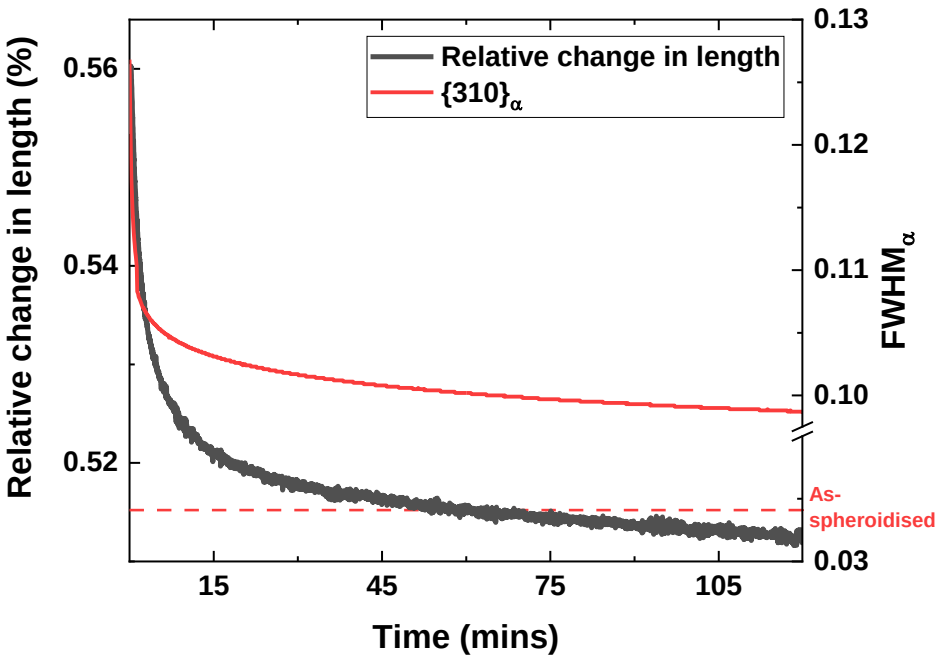
Relative change in length
{310}α
Relative change in length (%)
0.56
0.54
0.52
0.13
0.12
0.11
0.10
0.03
FWHMα
As-spheroidised
15
45
75
105
Time (mins)

Fig. 8

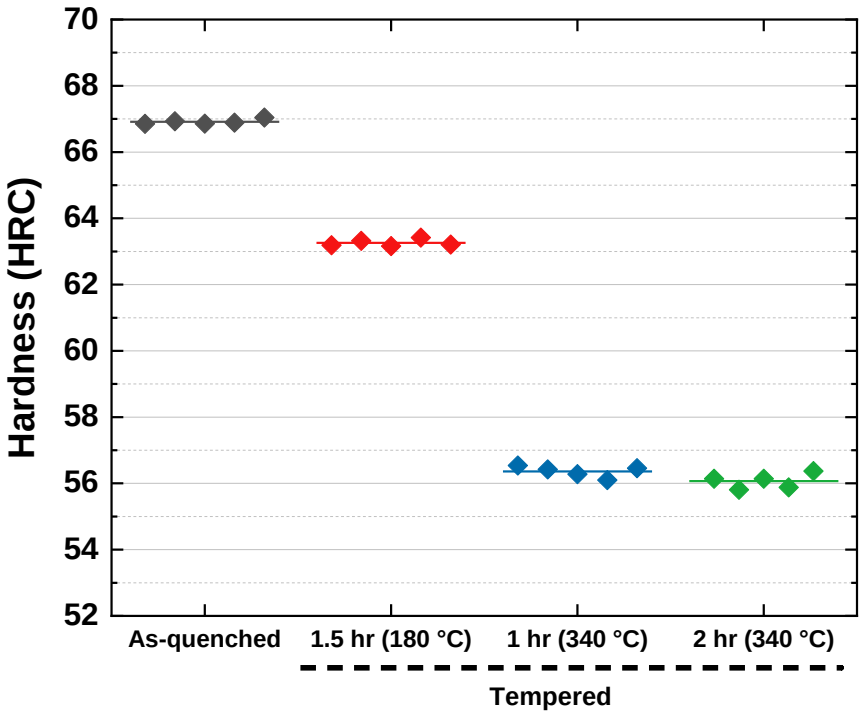
Hardness (HRC)
70
68
66
64
62
60
58
56
54
52
As-quenched
1.5 hr (180 °C)
1 hr (340 °C)
2 hr (340 °C)
Tempered

Fig. 9

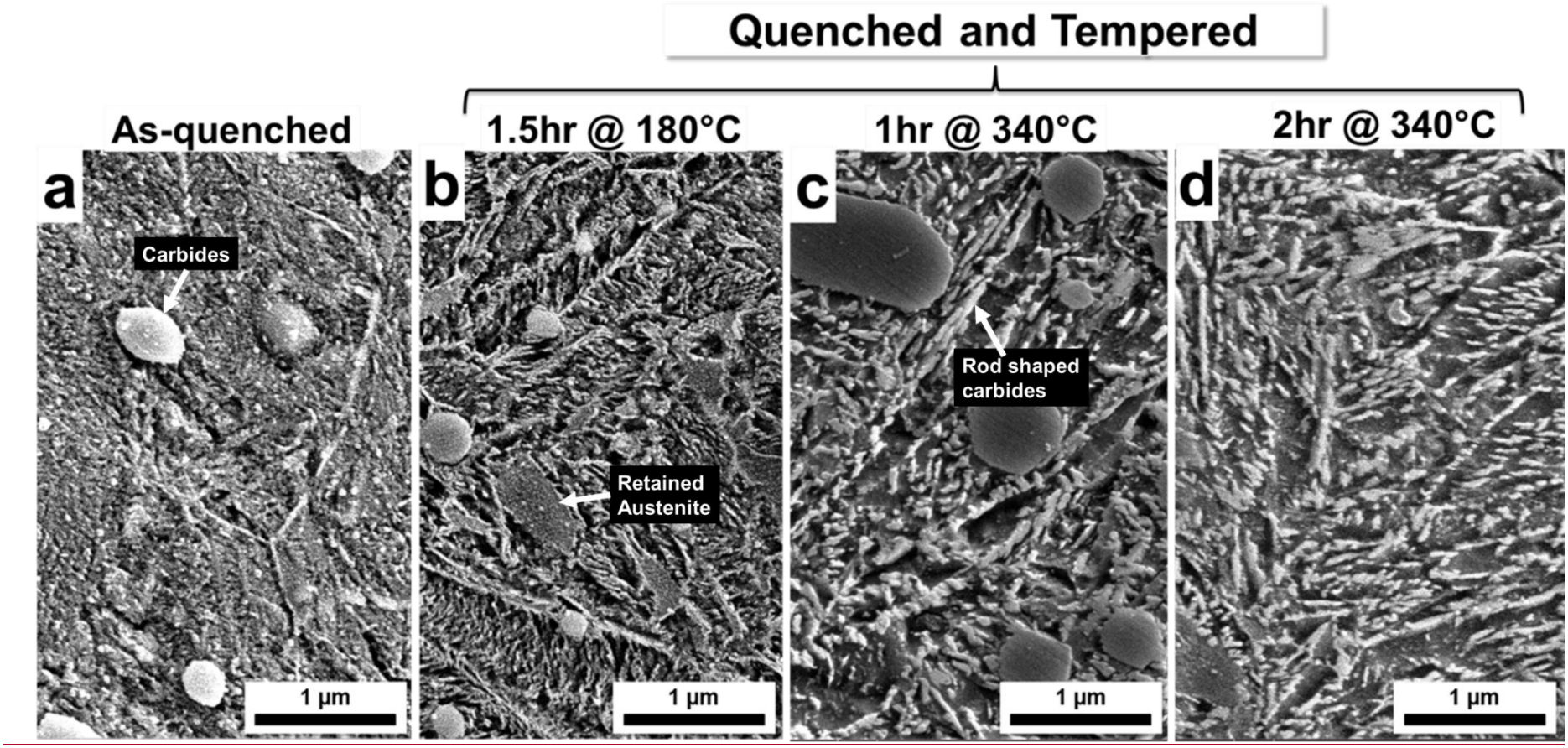
Quenched and Tempered
As-quenched
1.5hr @ 180°C
1hr @ 340°C
2hr @ 340°C
a
b
c
d
Carbides
Retained Austenite
Rod shaped carbides
1 µm
1 µm
1 µm
1 µm

Fig. 10

Supplementary material

In-situ synchrotron X-ray diffraction during quenching and tempering of SAE 52100 steel

D. Foster[a,1], M. Paladugu[b,2], J. Hughes[a], M. Kapousidou[a], U. Islam[a], A. Stark[c], N. Schell[c], E. Jimenez-Melero[a]

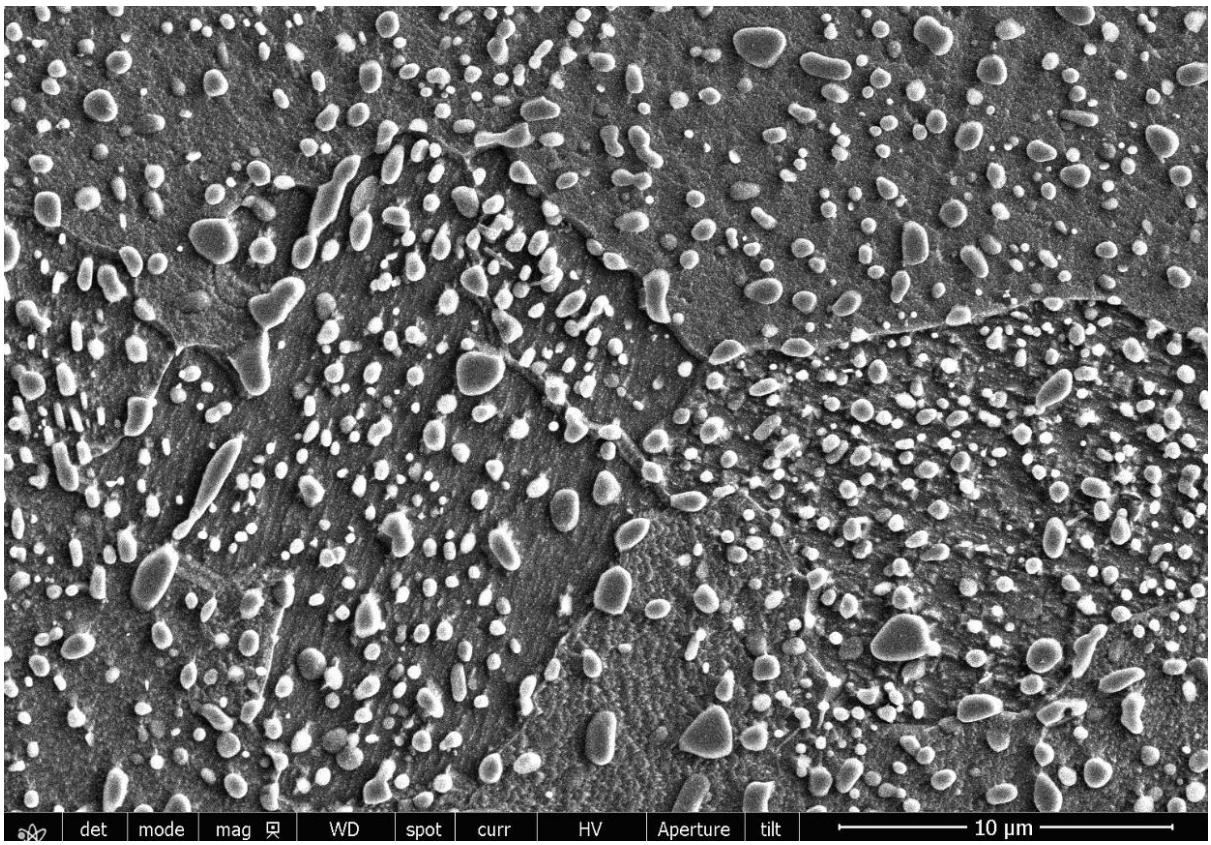

Fig. S1. The as-spheroidised starting microstructure of the SAE 52100 steel used in this study. The microstructure shows spheroidised carbide particles in ferrite matrix.

[1] daniel.foster-7@postgrad.manchester.ac.uk (DF)

[2] mohan.paladugu@timken.com (Mohan Paladugu)

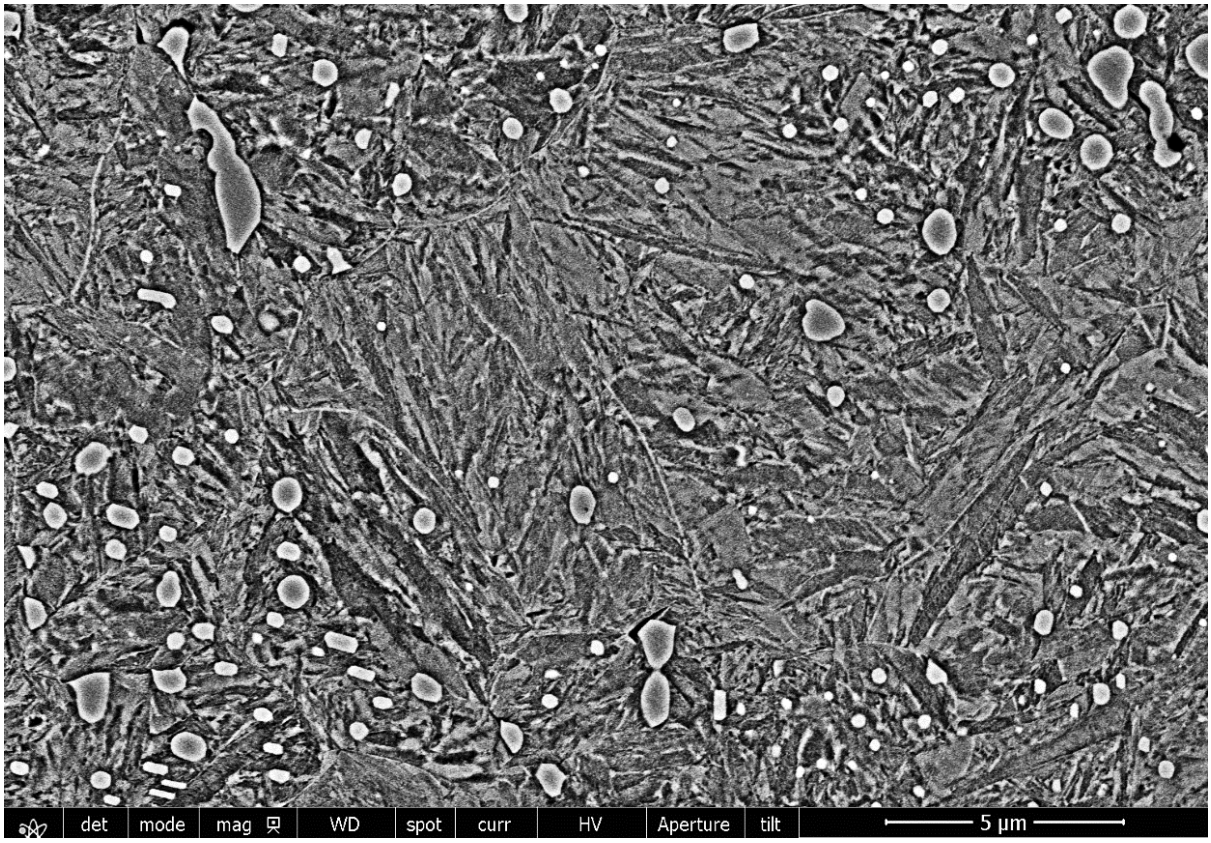

Fig. S2. SEM micrograph showing lath morphology of martensite in the as-quenched state of SAE 52100 steel.

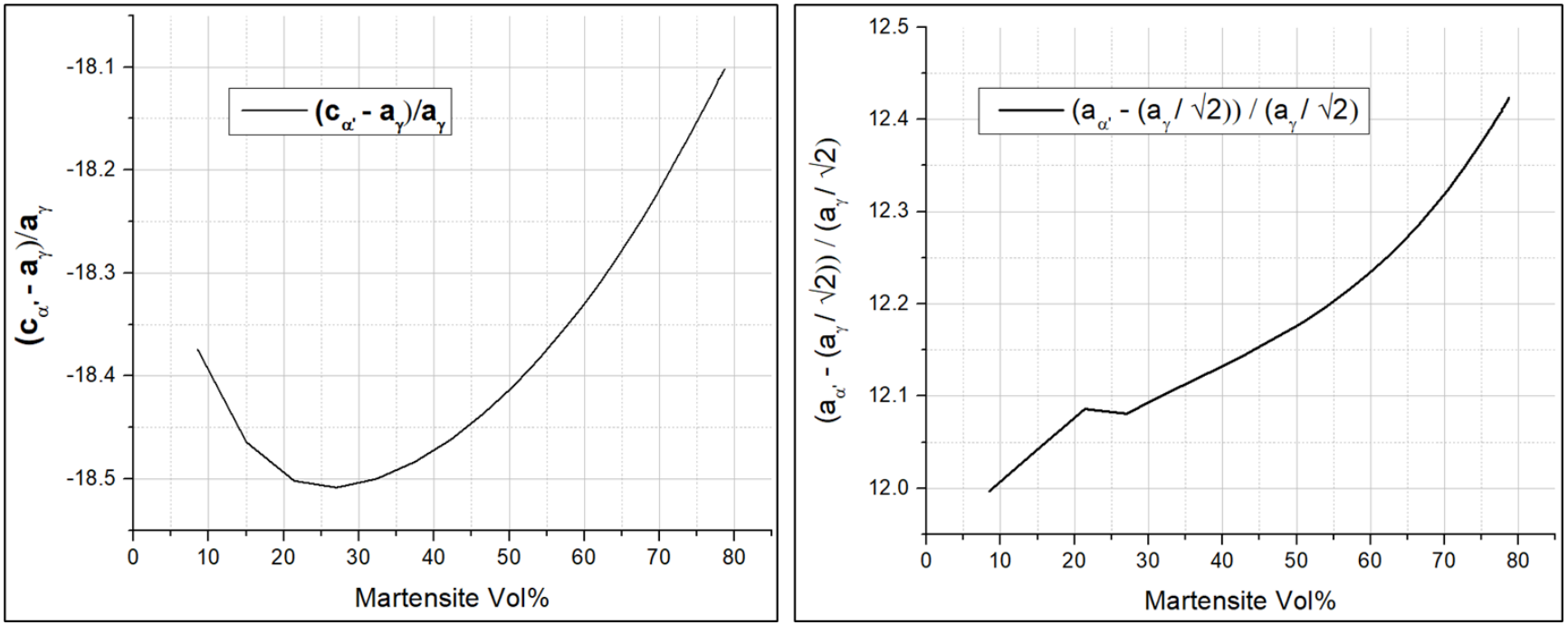

Fig. S3. Change in Bain strains as more martensite forms during quenching.

Declaration of interests

☒ The authors declare that they have no known competing financial interests or personal relationships that could have appeared to influence the work reported in this paper.

☐The authors declare the following financial interests/personal relationships which may be considered as potential competing interests:

D. Foster: Conceptualisation, methodology, formal analysis, investigation, writing – original and revised drafts, visualisation

M. Paladugu: Conceptualisation, resources, writing – review & editing, supervision

J. Hughes: investigation

M. Kapousidou: investigation

U. Islam: investigation

A. Stark: investigation

N. Schell: investigation

E. Jimenez-Melero: Conceptualisation, methodology, investigation, writing – review & editing, supervision